Positive and negative sequence currents optimization to improve voltages under unbalanced faults

Fill this

***Abstract*—Grid faults constitute a series of unfortunate events that compromise power systems. With the increasing integration of renewables and their associated power electronics converters, the injected currents are controllable, but at the same time, they have to be limited so as not to damage the semiconductors. This poses the challenge to determine the combination of currents that improves the most the voltages at the point of common coupling. In this paper, such an issue is approached from an optimization perspective. Solving the optimization problem allows comparing its solutions with respect to the ones obtained by following the grid code control laws. Two fundamental scenarios are presented: one with a single converter, and another with two converters. Several parameters are varied for all kinds of faults to spot the changes on the currents, such as the severity of the fault, the distance of a hypothetical submarine cable, and the resistive/inductive ratio of the impedances. Overall the results indicate that injecting only reactive power is not always the preferable choice. While grid codes are not optimal, they can be regarded as near-optimal decision rules.**

***Index Terms*—VSC, Grid-Support, Reference Optimization, Asymmetrical Fault, Current Saturation**

I. Introduction

THE rise in renewable energies has carried along with it the inclusion of Voltage Source Converters (VSC) as a means of coupling energetic resources to the grid while providing controllability [1]–[3]. Adopting such power electronics equipment has induced a progressive shrinkage on synchronous generators' influence in power systems. The high flexibility of VSC control enables advanced grid-support control, which could enhance the system performance during the fault and ensure a fast recovery after the fault clearance. However, compared to electrical machines, VSCs cannot withstand overloads [4]. Indeed, current (and also voltage) limitations cause VSC to behave differently. They reach what is called a saturated state. Many equilibrium points may arise as a result of that, especially in grids formed by multiple converters operating in critical conditions. The solution to such systems is also likely to become an arduous task to compute, as saturation states are defined by non-linear equations, or in more detail, by piecewise functions.

Not only do currents have to be constrained to not exceed the limitations, but they also have to collaborate on improving the voltages [5]. This becomes visible when looking at the requirements imposed by Transmission System Operators (TSO) in its grid codes [6], [7]. Although this was not the case years ago, when wind power represented a small percentage of the electricity mix, nowadays wind power plants have to control active and reactive power [8]. Besides, they have to transiently support the faults. The latter aspect is often referred to as low voltage ride through (LVRT) [9], [10]. The traditional approach to raise the voltage at the point of common coupling is to inject reactive power proportionally to the severity of the fault [8], [11]. During the analysis of faults, it is often the case that voltages are decomposed into positive, negative, and zero sequence values. By doing so, the study of the fault is expected to be simplified, and in addition to that, some intuition can be build from inspecting the positive and negative sequence voltages. A concerning unbalanced fault is such that substantially decreases the positive sequence voltage with respect to the nominal voltage while the negative sequence voltage increases. Both sequences have to be thoroughly controlled, as discussed in [11], [12].

Nevertheless, for the most part, grid codes only specify reactive power injection during faults [13], [14]. This is because transmission networks are often considered to have an inductive characteristic. The influence of the grid impedance characteristics of the system optimized under an equilibrium state is covered in [12], where the authors express the currents to inject as a function of the voltage and the impedances. A recursive relation between the voltage and the current is found, which invalidates the possibility of working with a closed-form expression from where to compute the optimal currents solution. Expressions of the same nature are proposed in [15], where instead of attempting to solve the optimization problem, a control parameter is introduced. This takes various values, but no analysis is carried out to determine the optimal choice. The effect of varying this control parameter is studied in [16], although it is not computed with a systematic approach, but rather, manually. Reference [17] proposes a maximum allowed support (MAS) control scheme that is said to provide the maximum voltage support and simultaneously satisfying the current limitations. The study does not explicitly indicate how the current is distributed among the real and the imaginary positive and negative sequence components, and variations in input parameters are rather limited. Another voltage support scheme is presented in [18], where the injected currents depend neither on the active power nor the filter resistance. In addition, positive and negative sequence grid voltage values are imposed, which facilitates the obtention of the steady-state current values. A variation of the grid code requirements is depicted in [19]. The authors found it to provide better results than conventional grid codes. The majority of the grid support strategies described above are compared and summarized in [20]. It is worth mentioning that the systems under study considered in these references include a single VSC. Further conclusions are expected to be extracted from examining a two-converter case study.

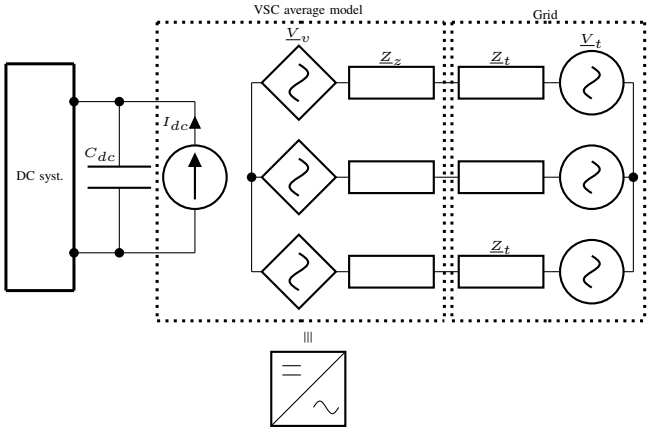

Fig. 1: Average model of a VSC connected to the grid

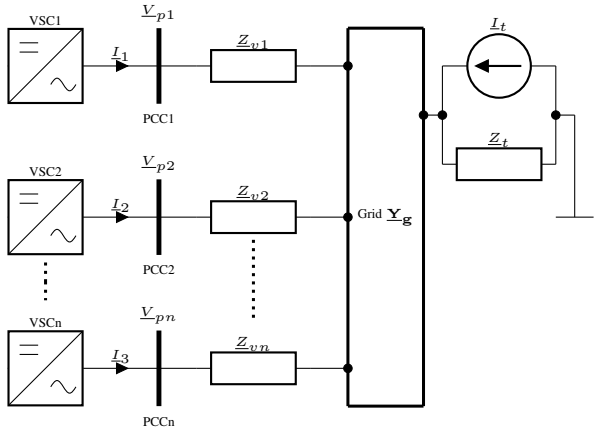

Fig. 2: Single-phase representation of a complete system

This paper proposes a methodology to identify the optimized system equilibrium point during the fault considering converters' current limitations. Two other control rules are implemented. One focuses on solving the optimization problem but in addition to the other constraints, it is restricted to only injecting reactive power. The third control rule follows the implementation of grid code specifications with its characteristic droop profile. These three options are tested for both balanced and unbalanced faults, where this last category includes the line to ground, the line to line, and the double line to ground faults. First, a basic system with a single converter is studied. Then, the analysis is repeated for a system with two converters in order to identify their interaction in saturated states.

Two main contributions come from this paper. On the one hand, it indicates the preferable injected currents under diverse conditions. A deeper understanding of the optimality of the solutions is expected to be gained from it. On the other hand, comparisons between the optimal solution and the one obtained by following the grid code are presented. An assessment about the convenience of grid codes to support faults can be derived, which should be useful when proposing future modifications in order to evolve towards more resilient grids.

II. Formulation

A. System modeling

VSCs are elements that interconnect DC systems with AC systems. As shown in Figure 1, they can be modeled following the so-called average model, where the switchings of the semiconductors are excluded. The VSC has been assumed to be connected to the AC grid with a filter in between denoted by $\underline{Z}_z$. The control strategy of the VSC consists of adjusting the voltages appropriately so that currents can indirectly meet the references [21].

Power systems are likely to involve more than a single converter. Therefore, the modeling is approached from a generalized perspective. Figure 2 presents the modeling for a system with n converters. They are connected to a grid which has been split into a passive part, only formed by impedances and denoted by its admittance matrix $\underline{\mathbf{Y}}_{\mathbf{g}}$, and an active part, modeled with a Norton equivalent. Compared to dealing with a Thevenin equivalent, the Norton equivalent simplifies the formulation since it does not create an additional bus. The VSCs are treated as current sources that inject currents of the form of $\underline{I}_k \forall k \in [1, ..., n]$. Additional impedances denoted by $\underline{Z}_{vk}$ connect the point of common coupling to the grid. Such point of common coupling is precisely where the voltages ought to be improved.

The relationship between currents and voltages can be established with an analysis in the natural reference frame or by employing symmetrical components as in [22]. Although both approaches are equally valid, working in the natural reference frame allows studying the system with greater flexibility, as only the particular elements of the admittance matrices that depend on the fault admittance experience changes. No other modifications in the topology have to be considered. Consequently, voltages and currents are related by

$$\begin{pmatrix} \underline{\mathbf{I}}_{\mathbf{1}} \\ \underline{\mathbf{I}}_{\mathbf{2}} \\ \vdots \\ \underline{\mathbf{I}}_{\mathbf{n}} \\ \underline{\mathbf{I}}_{\mathbf{t}} \end{pmatrix} = \begin{pmatrix} \underline{\mathbf{Y}}_{\mathbf{v1}} & \mathbf{0} & \dots & \mathbf{0} & -\underline{\mathbf{Y}}'_{\mathbf{v1}} \\ \mathbf{0} & \underline{\mathbf{Y}}_{\mathbf{v2}} & \dots & \mathbf{0} & -\underline{\mathbf{Y}}'_{\mathbf{v2}} \\ \vdots & \vdots & \ddots & \vdots & \vdots \\ \mathbf{0} & \mathbf{0} & \dots & \underline{\mathbf{Y}}_{\mathbf{vn}} & -\underline{\mathbf{Y}}'_{\mathbf{vn}} \\ -\underline{\mathbf{Y}}'^{\mathbf{T}}_{\mathbf{v1}} & -\underline{\mathbf{Y}}'^{\mathbf{T}}_{\mathbf{v2}} & \dots & -\underline{\mathbf{Y}}'^{\mathbf{T}}_{\mathbf{vn}} & \underline{\mathbf{Y}}_{\mathbf{g}} \end{pmatrix} \begin{pmatrix} \underline{\mathbf{V}}_{\mathbf{p1}} \\ \underline{\mathbf{V}}_{\mathbf{p2}} \\ \vdots \\ \underline{\mathbf{V}}_{\mathbf{pn}} \\ \underline{\mathbf{V}}_{\mathbf{g}} \end{pmatrix}. \tag{1}$$

For a given converter k, its injected currents and its associated voltages at the point of common coupling are further developed as

$$\begin{cases} \underline{\mathbf{I}}_{\mathbf{k}} = \left[\underline{I}_k^{(a)}, \underline{I}_k^{(b)}, \underline{I}_k^{(c)}\right]^T \\ \underline{\mathbf{V}}_{\mathbf{pk}} = [\underline{V}_{pk}^{(a)}, \underline{V}_{pk}^{(b)}, \underline{V}_{pk}^{(c)}]^T \end{cases} \tag{2}$$

i.e., they contain the a, b and c phase values. Voltages and currents are related via admittance matrices of the form $\underline{\mathbf{Y}}_{\mathbf{vk}}$, which in normal operating conditions follow

$$\underline{\mathbf{Y}}_{\mathbf{vk}} = \begin{pmatrix} \frac{1}{\underline{Z}_{vk}} & 0 & 0 \\ 0 & \frac{1}{\underline{Z}_{vk}} & 0 \\ 0 & 0 & \frac{1}{\underline{Z}_{vk}} \end{pmatrix}. \tag{3}$$

In case a fault occurs at the buses interconnected by $\underline{Z}_{vk}$, elements $1/\underline{Z}_f$ are added by observation, where $\underline{Z}_f$ denotes the fault impedance.

On the contrary, the admittance matrix $\underline{\mathbf{Y}}_{\mathbf{g}}$ is a $3n_g \times 3n_g$ matrix also built by observation. The object $\underline{\mathbf{I}}_{\mathbf{t}}$ is a vector of dimensions $3 \times n_g$ which accounts for the injected currents into the grid denoted by $\underline{\mathbf{Y}}_{\mathbf{g}}$. All its elements are null except for three entries that consider the injected currents from the Norton equivalent of the grid. Matrices of the form $\underline{\mathbf{Y}}'_{\mathbf{vk}}$ are $3 \times 3n_g$ objects constituted by elements $1/\underline{Z}_{vk}$. In a realistic scenario, the grid $\underline{\mathbf{Y}}_{\mathbf{g}}$ may be partially constitued by active and reactive power loads, i.e., PQ buses. They can be either ignored if the current they consume is assessed to be comparatively smaller than the fault current, or they can be modeled as constant admittances. No PQ loads have been considered in the case studies shown in this paper.

The final goal of the modeling is the obtention of voltages. They are computed from (1) by operating the product between the inverse of the full admittance matrix and the currents' vector. In order to have a clearer comprehension of the voltages, they are eventually converted into symmetrical components by means of Fortescue's transformation [23]:

$$\begin{pmatrix} \underline{V}^0_{pk} \\ \underline{V}^+_{pk} \\ \underline{V}^-_{pk} \end{pmatrix} = \frac{1}{3} \begin{pmatrix} 1 & 1 & 1 \\ 1 & a & a^2 \\ 1 & a^2 & a \end{pmatrix} \begin{pmatrix} \underline{V}^a_{pk} \\ \underline{V}^b_{pk} \\ \underline{V}^c_{pk} \end{pmatrix} \ , \tag{4}$$

where $a = e^{j\frac{2\pi}{3}}$.

B. Optimization problem

Positive sequence voltages have to be maximized while negative sequence voltages have to be minimized. The zero sequence component of the voltages is a magnitude likely to become non-null under asymmetrical faults. Nevertheless, as VSC are unable to inject zero sequence currents, it will remain an uncontrolled variable in the sense that no efforts will be made towards reducing it. Current saturation restrictions imposed by the VSC characteristics have to be respected. This applies to each phase of each converter. Therefore, the generic optimization problem is

$$\begin{aligned} \min_{\underline{I}} \quad & \sum_{k=1}^{n} \left[\lambda^+_k |(1 - |\underline{V}^+_{pk}(\underline{I})|)| + \lambda^-_k |(0 - |\underline{V}^-_{pk}(\underline{I})|)| \right] \ , \\ \text{s.t.} \quad & \max(\underline{I}^a_k, \underline{I}^b_k, \underline{I}^c_k) \leq I_{\text{max,k}} \ \forall k \in [1, ..., n] \ , \\ & \underline{I}^a_k + \underline{I}^b_k + \underline{I}^c_k = 0 \ \forall k \in [1, ..., n] \ , \end{aligned} \tag{5}$$

where the positive and negative sequence components of voltages $\underline{V}_{pk}$ are symbolically expressed as functions of the currents, and $I_{\text{max,k}}$ is the maximum allowed current by the k converter. It has been assumed that voltages at each phase of the converter do not surpass the limitations, which seems a fair assumption considering that voltages decreases substantially during faults. Ignoring voltage limitations tends to be a commonality in the literature as well.

The results gathered in this paper are computed with Python 3.9.1 and the aid of the Mystic package, a highly-constrained non-convex optimization framework [24], [25]. A differential global optimization solver has been employed with a relative precision up to $1e-6$.

C. Grid code rules

In order to improve voltages during faults, grid code control rules typically impose injections of currents proportional to the voltage drop [8], [26]. When defined as piecewise functions, for the positive sequence

$$\begin{cases} |\underline{I}^+_k| = 0 & |\underline{V}^+_{pk}| \geq 0.9 \\ |\underline{I}^+_k| = k_p(0.9 - |\underline{V}^+_{pk}|) & 0.4 \leq |\underline{V}^+_{pk}| < 0.9 \\ |\underline{I}^+_k| = I_{\text{max},k} & |\underline{V}^+_{pk}| < 0.4 \end{cases} \tag{6}$$

whereas for the negative sequence

$$\begin{cases} |\underline{I}^-_k| = 0 & |\underline{V}^-_{pk}| \leq 0.1 \\ |\underline{I}^-_k| = k_n(|\underline{V}^-_{pk}| - 0.1) & 0.1 \leq |\underline{V}^-_{pk}| < 0.6 \\ |\underline{I}^-_k| = I_{\text{max},k} & |\underline{V}^-_{pk}| > 0.6 \end{cases} \tag{7}$$

Both constants k_p and k_n are set at $1.25 I_{\text{max},k}$. This value was empirically found to be large enough so that currents approached the limitations without exceeding them.

The application of the grid code rules implies that maximum phase currents are hardly ever equal to the maximum allowed by the VSC, even when strong faults occur. Thus, an adaptative control can be formulated so that currents tend to the maximum permitted value while the droop characteristic is preserved. This strategy is denoted by ADA, as in essence it consists of an adaptative mechanism. In order to fairly compare between methodologies, k_p and k_n are always equal. A central goal of this paper is concerned with determining beforehand the value of $k_p = k_n$, i.e., independently of fault voltages.

D. Summary of support techniques

The paper evaluates and compares three support strategies, which are:

- OPT: corresponds to the solution of the optimization problem in (5), particularized for each system. It provides, by definition, the best solution.
- GC: is the application of the grid code rules shown in (6) and (7), with $k_p = k_n = 1.25$. It should generate the less convenient solution out of the three analyzed strategies.
- ADA: mimics the grid code rules from (6) and (7) with an adapted value of the constants $k_p = k_n$ so that the VSC operates close to the current limitations.

III. Single converter case study

The analysis is first performed considering a one-converter case study as the one depicted in Figure 3. A fault is caused at the point of connection of the grid. The impedances that model the fault are set accordingly to the type of fault, i.e., balanced or unbalanced (line to ground, line to line or double line to ground). The goal is to improve the voltage $\underline{V}_{p1}$ by injecting the optimal $\underline{I}^a_1$, $\underline{I}^b_1$ and $\underline{I}^c_1$ currents.

Three parametric studies are performed. One considers variations in the fault impedance. This case is explicitly described in order to exemplify the formulation. Another study analyzes a varying R_1/X_1 ratio, i.e., the proportion between the resistive and the inductive parts that compose the

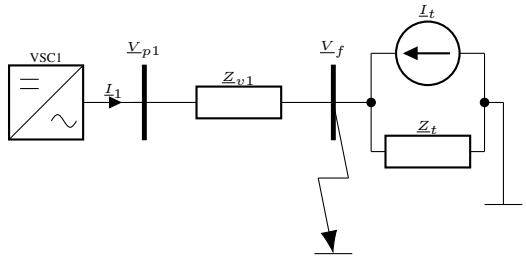

Fig. 3: Single-phase representation of the single converter system under study

impedance $\underline{Z}_{v1}$ is modified while the absolute value of the impedance is kept constant. The third case presents the effect of increasing the distance of a hypothetical submarine cable.

A. Fault impedance variation analysis

For a single converter system as the one depicted in Figure 3, the fault impedance connected to the bus at voltage $\underline{V}_f$ is responsible for identify the fault. Explicitly, voltages and currents are related by

$$\begin{pmatrix} \underline{I}_1^a \\ \underline{I}_1^b \\ \underline{I}_1^c \\ \underline{I}_t^a \\ \underline{I}_t^b \\ \underline{I}_t^c \end{pmatrix} = (\underline{\mathbf{Y}}_\mathbf{v} + \underline{\mathbf{Y}}_\mathbf{f}) \begin{pmatrix} \underline{V}_{p1}^a \\ \underline{V}_{p1}^b \\ \underline{V}_{p1}^c \\ \underline{V}_f^a \\ \underline{V}_f^b \\ \underline{V}_f^c \end{pmatrix}, \tag{8}$$

where the admittance matrix has been split into two parts: $\underline{\mathbf{Y}}_\mathbf{v}$ represents the non-faulted admittance matrix of the system, whereas $\underline{\mathbf{Y}}_\mathbf{f}$ is constitued by the admittances that intervene in the fault. This way, the admittance matrices are defined as

$$\underline{\mathbf{Y}}_\mathbf{v} = \begin{pmatrix} \underline{Y}_{v1} & 0 & 0 & -\underline{Y}_{v1} & 0 & 0 \\ 0 & \underline{Y}_{v1} & 0 & 0 & -\underline{Y}_{v1} & 0 \\ 0 & 0 & \underline{Y}_{v1} & 0 & 0 & -\underline{Y}_{v1} \\ -\underline{Y}_{v1} & 0 & 0 & \underline{Y}_{v1}+\underline{Y}_t & 0 & 0 \\ 0 & -\underline{Y}_{v1} & 0 & 0 & \underline{Y}_{v1}+\underline{Y}_t & 0 \\ 0 & 0 & -\underline{Y}_{v1} & 0 & 0 & \underline{Y}_{v1}+\underline{Y}_t \end{pmatrix} \tag{9}$$

where $\underline{Y}_{v1} = 1/\underline{Z}_{v1}$ and $\underline{Y}_t = 1/\underline{Z}_t$.

On the other hand, the fault admittance $\underline{\mathbf{Y}}_\mathbf{f}$ is fully dependent on the fault and therefore, it is built by observation. The optimization problem for the one case converter reads

$$\begin{aligned} \min_{\underline{I}_1^a, \underline{I}_1^b, \underline{I}_1^c} \quad & \lambda_1^+ |(1 - |\underline{V}_{p1}^+(\underline{I}_1^a, \underline{I}_1^b, \underline{I}_1^c)|)| \\ & + \lambda_1^- |(0 - |\underline{V}_{p1}^-(\underline{I}_1^a, \underline{I}_1^b, \underline{I}_1^c)|)| \ , \\ \text{s.t.} \quad & \max(\underline{I}_1^a, \underline{I}_1^b, \underline{I}_1^c) \leq I_{\text{max},1} \ , \\ & \underline{I}_1^a + \underline{I}_1^b + \underline{I}_1^c = 0 \ , \end{aligned} \tag{10}$$

The procedure to solve the optimization problem is first responsible for initializing the admittances matrices $\underline{\mathbf{Y}}_\mathbf{v}$ as in (9), and then, constructing $\underline{\mathbf{Y}}_\mathbf{f}$. Next, currents are initialized to a random array of values, for instance. The Mystic package is subsequently called to solve the optimization problem stated in (10) up to a given relative precision δ, being $\delta = 1e-6$ for example. Positive and negative sequence voltages are evaluated to determine the optimality of the solution by means of (4). In case of sweeping a range of n scenarios, this process is repeated n times. Currents are eventually also transformed to positive and negative sequence values, since the final goal is to evaluate their values in this frame of reference. Unless noted otherwise, the corresponding baseline parameters of the system in Figure 3 are indicated in Table I.

TABLE I: System parameters for the one-converter case

Parameter	Value
$\underline{V}_t$	1.00
I_{max}	1.00
$\underline{Z}_{v1}$	$0.01 + j0.05$
$\underline{Z}_t$	$0.01 + j0.1$
$[\lambda_1^+, \lambda_1^-]$	$[1, 1]$

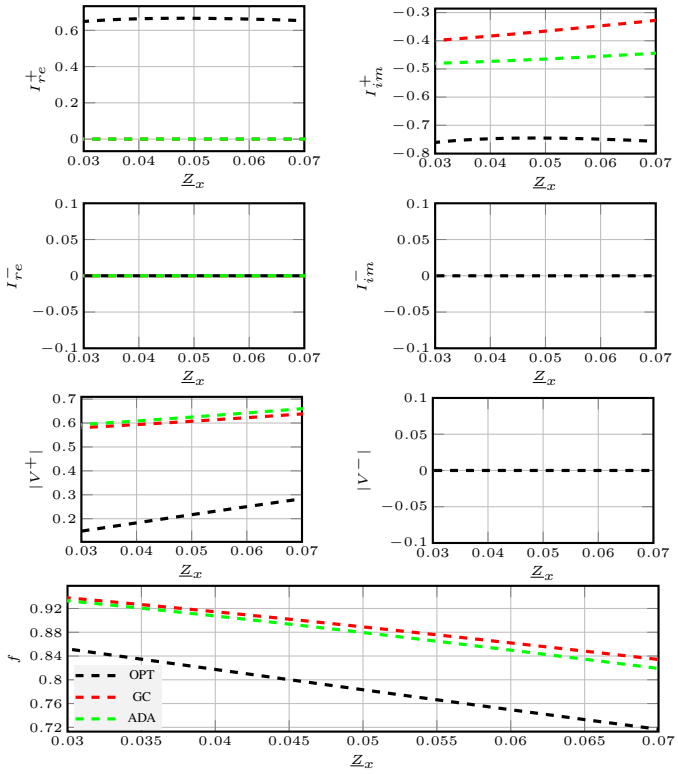

Fig. 4: Influence of the currents on the objective function for the balanced fault with a varying fault admittance, one converter case

Solving the problem with the aforementioned steps for a balanced fault yields the results shown in Figure 4, where impedance $\underline{Z}_x$ denotes the fault impedance connected to each phase. The results suggest that the OPT case is the preferred one, as its associated objective function is always the smallest, as expected. This optimal solution is achieved by distributing the currents between the real and imaginary parts. The current capabilities are roughly equally attributed among both. The ADA solution and the GC one present only slight differences, so varying the slope of the grid code current definitions does not yield remarkable benefits. However, this consitutes a particular scenario since no negative sequence current ought to be injected. The only difference between ADA and GC is that the former specifies a moderately higher current.

Significantly different results are obtained in the case of a line to line fault, as shown in Figure 5. This unbalanced fault

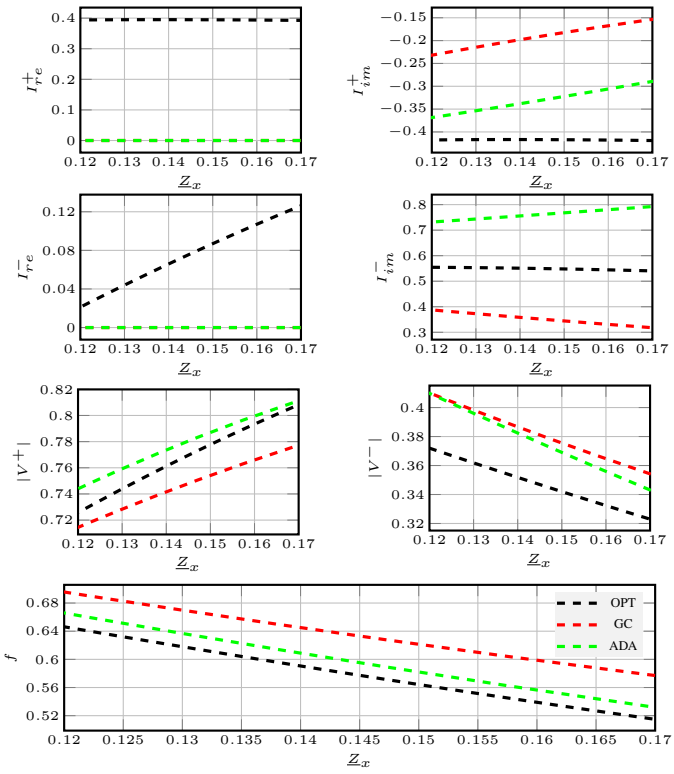

Fig. 5: Influence of the currents on the objective function for the line to line with a varying fault admittance, one converter case

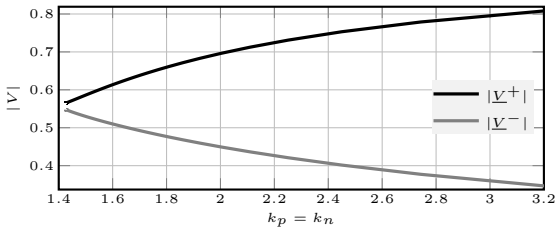

Fig. 6: Dependence between constants $k_p = k_n$ and the sequence voltages in the ADA approach for a line to line fault

causes the optimal currents to be non-null for the imaginary part of the negative sequence. While the OPT solution specifies almost constant current values in I^+_{re}, I^+_{im} and I^-_{im}, much more varying currents are injected in the case of ADA and GC. Thanks to the adaptative control, both I^+_{im} and I^-_{im} are larger than in the GC situation. Consequently, more voltage support is provided, which causes ADA to be a near-optimal solution despite not injecting any active power, specially for large values of $\underline{Z}_x$.

In essence, ADA does not retain the same linear droop characteristics than the GC rules defined in (6) and (7). Figure 6 shows the coupling between the constants $k_p = k_n$ and the positive and negatives sequence voltages for a line to line fault with $\underline{Z}_x \in [0.005, 0.17]$. The evolutions are quadratic, which suggests that a linear dependence between injected sequence currents and voltages would not result in near-optimal operating points.

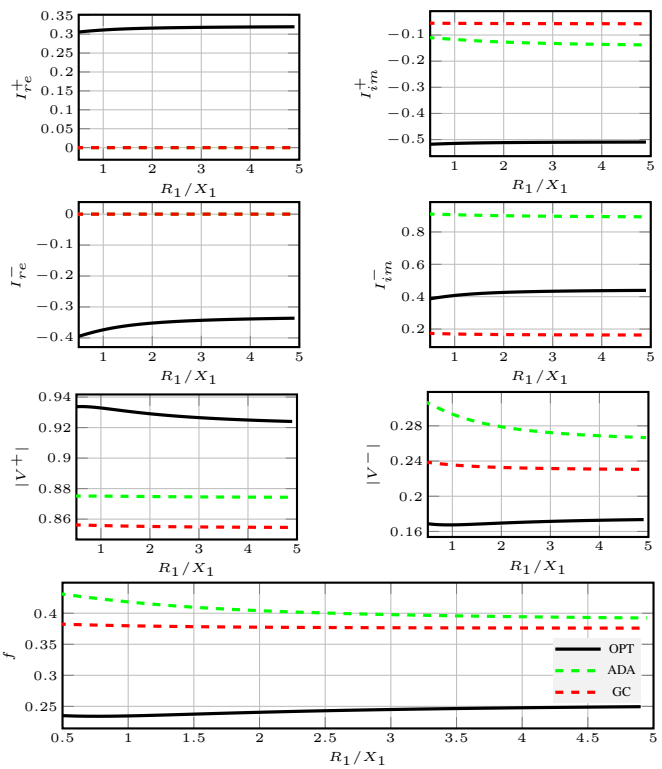

Fig. 7: Influence of the currents on the objective function for the line to ground fault with a varying R_1/X_1 ratio and $\underline{Z}_{ag} = 0.1$

B. R_1/X_1 variation analysis

The R_1/X_1 variation analysis performs a swept for a range of a varying angle of the $\underline{Z}_{v1}$ impedance, while the absolute value is preserved. The imaginary part of the currents (reactive component) tends to be superior than the real part (active component) for a small R_1/X_1 ratio. The currents evolve asymptotically, in the sense that even if the resistive part of the impedance is substantially larger than the reactance, the same prioritization applies. The ADA strategy dedicates most of its current capability to inject negative sequence reactive current, whereas the optimal solution tends to balance the currents not only between sequences but also between real and imaginary parts. Although ADA injects larger currents (by definition the saturation is forced), it does not provide a more favorable solution that the classical grid code GC. Differences are small, yet operating the VSC at its maximum current capabilities has a detrimental effect on the negative sequence voltage.

Noticeably, the objective function is further minimized in the OPT case. In percentual terms there is an approximate 40% improvement with respect to the GC approach. This is achieved balancing the currents. When the VSC operates at the optimal conditions, it takes full advantage of the current capabilities, just like it happened in the line to line fault shown in Figure 5. Thus, a line to ground fault with a predominant resistive characteristic is much more prone to being improved by means of adequately distributing the currents across sequences and real/imaginary parts. Across all range of R_1/X_1 values analyzed in Figure 7, the injected active power remains

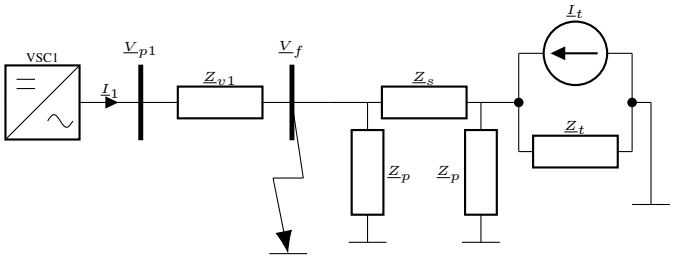

Fig. 8: Single-phase representation of the single converter connected to a system with a cable

TABLE II: System parameters for the one-converter case

Parameter	Value	Units
$\underline{Z}_s$	$6.674 \cdot 10^{-5} + j2.597 \cdot 10^{-4}$	pu/km
$\underline{Z}_p$	$-j77.372$	pu·km

between 0.405 and 0.401 whereas the reactive power is around 0.486 to 0.461. In short, the injection of active power has a positive contribution.

C. Cable length variation analysis

Figure 8 represents a third case regarding single converter systems, which deals with a hypothetical submarine cable modeled with its π equivalent. The data selected to model the cable are extracted from [27] and adapted to per unit values. Table II presents them. The followed approach to analyze the system is identical to the previous ones, except for the reduction of the set of elements including the cable and the grid. The corresponding Thevenin equivalent is defined by

$$\begin{cases} \underline{V}'_t = \frac{\underline{Z}_p \underline{Z}_p}{2\underline{Z}_t\underline{Z}_p + \underline{Z}_p\underline{Z}_s + \underline{Z}_p\underline{Z}_p + \underline{Z}_t\underline{Z}_s} \\ \underline{Z}'_t = \frac{\underline{Z}_p\underline{Z}_p\underline{Z}_t + \underline{Z}_p\underline{Z}_p\underline{Z}_s + \underline{Z}_p\underline{Z}_s\underline{Z}_t}{2\underline{Z}_p\underline{Z}_t + \underline{Z}_s\underline{Z}_p + \underline{Z}_s\underline{Z}_t + \underline{Z}_p\underline{Z}_p} \end{cases} \tag{11}$$

Similarly as before, a Norton equivalent is preferred. The current $\underline{I}'_t$ is simply equal to $\underline{V}'_t/\underline{Z}'_t$, which yields a basic system as the one in Figure 3.

The analysis performed considers a cable with a varying length, up to 75 km. Its impact on the Thevenin equivalent parameters is shown in Figure 9. The voltage experiences a subtle increase, while the imaginary part of the equivalent impedance grows considerably with distance, yet the $\Re(\underline{Z}'_t)/\Im(\underline{Z}'_t)$ ratio tends to rise.

The cases OPT, ADA and GC are again evalauted, as depicted in Figure 10. The OPT situation unveils that, contrary

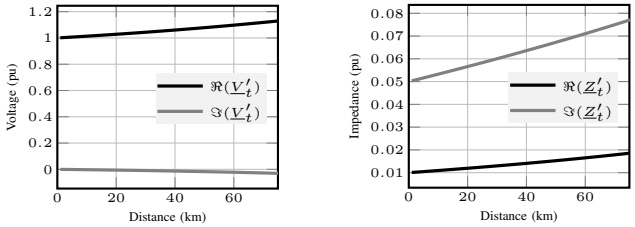

Fig. 9: Influence of the cable distance on the Thevenin voltage and impedance

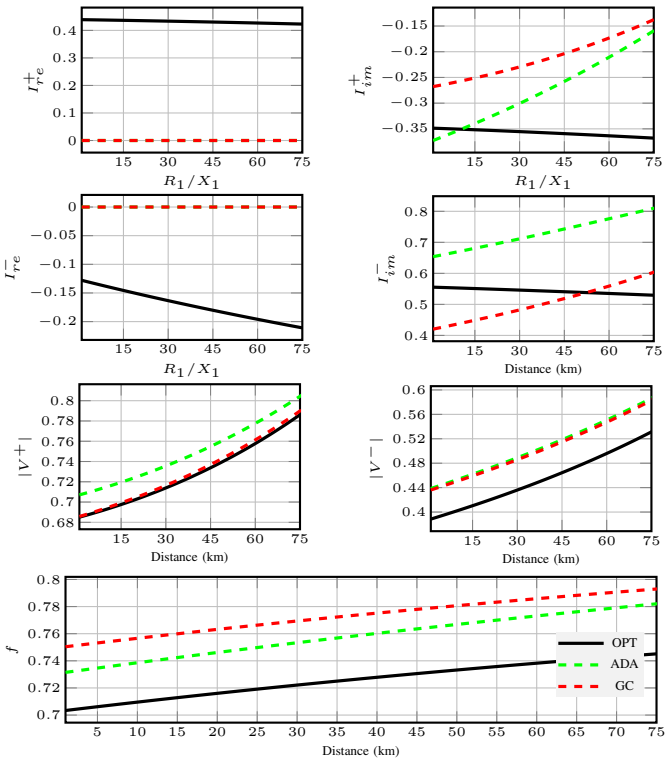

Fig. 10: Influence of the currents on the objective function for a line to line fault with a varying cable distance

to ADA and GC, imaginary currents ought to be rather stable. While in practical terms its positive sequence voltage is the same as the one from the standard grid code (GC), the negative sequence voltage becomes about 10% lower. Therefore it can be stated that the optimization yields the most favorable value in general terms, although as it is the case here, some sequence may be worse off than the other options. Compared to GC, ADA maximizes the positive sequence voltage mainly by injecting larger negative sequence imaginary currents. However, an improvement of about 2% in the objective function may not justify operating the converter at its maximum current capabilities.

Increasing the cable distance causes the negative sequence voltage to grow, while the positive sequence voltage also tends to grow. This phenomena differs from the profiles obtained in Figures 5 and 7, where both voltages either simultaneously approached the objective value (1 and 0 respectively), or distanced from it.

IV. Two converter case study

Fill this

A. Fault impedance variation analysis

B. R/X variation analysis

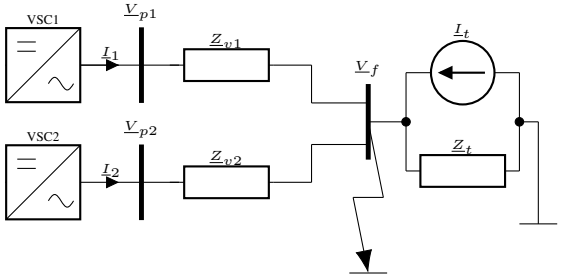

Fig. 11: Single-phase representation of the two-converter system under study

TABLE III: System parameters for the two converter case

Parameter	Value
$\underline{V}_t$	1.00
I_{max}	1.00
$\underline{Z}_{v1}$	$0.01 + j0.05$
$\underline{Z}_{v2}$	$0.01 + j0.06$
$\underline{Z}_t$	$0.01 + j0.1$
$[\lambda_1^+, \lambda_1^-, \lambda_2^+, \lambda_2^-]$	$[1, 1, 1, 1]$

V. ////////////PLOTS////////////

VI. Conclusion

Fill this

Acknowledgment

Fill this.

References

[1] M. Imhof and G. Andersson, "Power system stability control using voltage source converter based hvdc in power systems with a high penetration of renewables," in *2014 Power Systems Computation Conference*. IEEE, 2014, pp. 1–7.

[2] S. Eren, A. Bakhshai, and P. Jain, "Control of three-phase voltage source inverter for renewable energy applications," in *2011 IEEE 33rd International Telecommunications Energy Conference (INTELEC)*. IEEE, 2011, pp. 1–4.

[3] F. Blaabjerg, Y. Yang, K. Ma, and X. Wang, "Power electronics-the key technology for renewable energy system integration," in *2015 International Conference on Renewable Energy Research and Applications (ICRERA)*. IEEE, 2015, pp. 1618–1626.

[4] A. Abdou, A. Abu-Siada, and H. Pota, "Improving the low voltage ride through of doubly fed induction generator during intermittent voltage source converter faults," *Journal of Renewable and Sustainable Energy*, vol. 5, no. 4, p. 043110, 2013.

[5] J. Morren, *Grid support by power electronic converters of Distributed Generation units*, 2006.

[6] I. Erlich, W. Winter, and A. Dittrich, "Advanced grid requirements for the integration of wind turbines into the german transmission system," in *2006 IEEE Power Engineering Society General Meeting*. IEEE, 2006, pp. 7–pp.

[7] X. Zhang, Z. Wu, M. Hu, X. Li, and G. Lv, "Coordinated control strategies of vsc-hvdc-based wind power systems for low voltage ride through," *energies*, vol. 8, no. 7, pp. 7224–7242, 2015.

[8] M. Mohseni and S. M. Islam, "Review of international grid codes for wind power integration: Diversity, technology and a case for global standard," *Renewable and Sustainable Energy Reviews*, vol. 16, no. 6, pp. 3876–3890, 2012.

[9] M. Tsili and S. Papathanassiou, "A review of grid code technical requirements for wind farms," *IET Renewable power generation*, vol. 3, no. 3, pp. 308–332, 2009.

[10] J. Conroy and R. Watson, "Low-voltage ride-through of a full converter wind turbine with permanent magnet generator," *IET Renewable power generation*, vol. 1, no. 3, pp. 182–189, 2007.

[11] A. Haddadi, I. Kocar, J. Mahseredjian, U. Karaagac, and E. Farantatos, "Negative sequence quantities-based protection under inverter-based resources challenges and impact of the german grid code," *Electric Power Systems Research*, vol. 188, p. 106573, 2020.

[12] A. Camacho, M. Castilla, J. Miret, L. G. de Vicuña, and R. Guzman, "Positive and negative sequence control strategies to maximize the voltage support in resistive–inductive grids during grid faults," *IEEE Transactions on Power Electronics*, vol. 33, no. 6, pp. 5362–5373, 2017.

[13] Red Eléctrica de España. (2016) Información sobre implementación de códigos de red de conexión. textos de los códigos de red de conexió europeos. reglamento 2016/631. [Online]. Available: https://www.esios.ree.es/es/pagina/codigos-red-conexion

[14] A. G. Paspatis and G. C. Konstantopoulos, "Voltage support under grid faults with inherent current limitation for three-phase droop-controlled inverters," *Energies*, vol. 12, no. 6, p. 997, 2019.

[15] A. Camacho, M. Castilla, J. Miret, J. C. Vasquez, and E. Alarcon-Gallo, "Flexible voltage support control for three-phase distributed generation inverters under grid fault," *IEEE transactions on industrial electronics*, vol. 60, no. 4, pp. 1429–1441, 2012.

[16] X. Guo, X. Zhang, B. Wang, W. Wu, and J. M. Guerrero, "Asymmetrical grid fault ride-through strategy of three-phase grid-connected inverter considering network impedance impact in low-voltage grid," *IEEE Transactions on Power Electronics*, vol. 29, no. 3, pp. 1064–1068, 2013.

[17] M. M. Shabestary and Y. A.-R. I. Mohamed, "An analytical method to obtain maximum allowable grid support by using grid-connected converters," *IEEE Transactions on Sustainable Energy*, vol. 7, no. 4, pp. 1558–1571, 2016.

[18] Z. Dai, H. Lin, H. Yin, and Y. Qiu, "A novel method for voltage support control under unbalanced grid faults and grid harmonic voltage disturbances," *IET power Electronics*, vol. 8, no. 8, pp. 1377–1385, 2015.

[19] M. M. Shabestary and Y. A.-R. I. Mohamed, "Asymmetrical ride-through and grid support in converter-interfaced dg units under unbalanced conditions," *IEEE Transactions on Industrial Electronics*, vol. 66, no. 2, pp. 1130–1141, 2018.

[20] M. M. Shabestary, S. Mortazavian, and Y. I. Mohamed, "Overview of voltage support strategies in grid-connected vscs under unbalanced grid faults considering lvrt and hvrt requirements," in *2018 IEEE International Conference on Smart Energy Grid Engineering (SEGE)*. IEEE, 2018, pp. 145–149.

[21] M. T. Andani, H. Pourgharibshahi, Z. Ramezani, and H. Zargarzadeh, "Controller design for voltage-source converter using lqg/ltr," in *2018 IEEE texas power and energy conference (TPEC)*. IEEE, 2018, pp. 1–6.

[22] M. G. Taul, S. Golestan, X. Wang, P. Davari, and F. Blaabjerg, "Modeling of converter synchronization stability under grid faults: The general case," *IEEE Journal of Emerging and Selected Topics in Power Electronics*, 2020.

[23] C. L. Fortescue, "Method of symmetrical co-ordinates applied to the solution of polyphase networks," *Transactions of the American Institute of Electrical Engineers*, vol. 37, no. 2, pp. 1027–1140, 1918.

[24] M. M. McKerns, L. Strand, T. Sullivan, A. Fang, and M. A. Aivazis, "Building a framework for predictive science," *arXiv preprint arXiv:1202.1056*, 2012.

[25] M. McKerns, P. Hung, and M. Aivazis, "mystic: highly-constrained non-convex optimization and uq, 2009."

[26] National Grid, "The grid code, issue 6, revision 1," https://www.nationalgrideso.com/document/162271/download, 2021.

[27] M. Cheah, "Offshore wind integration through high voltage direct current systems," Ph.D. dissertation, Cardiff University, 2017.